IOP Conference Series:
Materials Science and
Engineering

PURPOSE-LED
PUBLISHING™

PAPER • **OPEN ACCESS**

Astigmatism Quantification for Depth Localization of Bubbles and Tracers across Curved Surfaces

To cite this article: H Lange *et al* 2024 *IOP Conf. Ser.: Mater. Sci. Eng.* **1322** 012005

View the article online for updates and enhancements.

You may also like

- Exploring the Potential of High-Fatty Acid Content Oils for Biodiesel Production: A Catalyst-Free Approach
MD Solikhah, SS Wirawan, AT Sugiarto et al.
- Preparation and application of waste cigarette butts-derived mulch film with excellent mechanical properties and optical transparency
Xianjie Liu, Sijun Huang, Genrong Li et al.
- Unidirectional fibre reinforcement of syntactic metal foams
B Szovák, J E Maróti, A Kemény et al.

This content was downloaded from IP address 141.52.248.2 on 04/03/2025 at 13:54

IOP Conf. Series: Materials Science and Engineering **1322** (2024) 012005 doi:10.1088/1757-899X/1322/1/012005

Astigmatism Quantification for Depth Localization of Bubbles and Tracers across Curved Surfaces

H Lange[1], **C Sax**[1], **A Brümmer**[2] and **J Kriegseis**[1*]

[1] Institute of Fluids Mechanics, Karlsruhe Institute of Technology, Karlsruhe, Germany

[2] Chair of Fluidics, TU Dortmund University, Dortmund, Germany

E-mail: kriegseis@kit.edu

Abstract. The present combined theoretical/experimental study addresses the impact of astigmatism on the two-phase flow diagnostics across the curved surfaces of liquid test-rig containments. In the present context, the target application is the two phase leakage-flow diagnostics across the annular housing gaps of oil-injected rotary positive displacement compressors (RPDC). Earlier studies by the authors identified the Defocusing Particle Tracking Velocimetry (DPTV) and Interferometric Particle Imaging (IPI) as particularly promising combination of flow measurement techniques to investigate the liquid and disperse gas phases inside the annular housing gap of RPDCs. The test-rig-specific influence of astigmatism on the resulting optical transfer function for a quantitative evaluation of the recorded defocused particle images (PI) is first compared to the theoretically derived circular PI diameter upon pure defocussing and subsequently tested for both classes of PIs, i.e DPTV and IPI. To mimic the optical configuration of optically accessible lateral surfaces of typical RPDC test rigs, a circular beaker glass (CBG) of comparable diameter is chosen for the experimental campaign. The results are discussed and future efforts for advanced PI-evaluation strategies are outlined on the grounds of the drawn conclusions.

1. Introduction

In order to increase the efficiency of rotary positive displacement compressors (RPDCs), an in-depth knowledge of the two-phase surge and gap flow between two adjacent compressor chambers is crucial as recently elaborated by e.g. Nikolov & Brümmer [1]. In addition to the measurement of torque the accordingly required experimental investigations moreover rely on the non-trivial flow measurement of both liquid and gas phases in the annular housing gap of the RPDCs. Such gap-flow investigations largely center around (laser-)optical imaging techniques, which either address the qualitative characterization of the spatio-temporal two-phase flow behavior or furthermore aim at a quantitative evaluation of velocity information inside the RPDC.

Xin *et al.* [2] and Vasuthevan & Brümmer [3], for instance, addressed the interrelationship of influential factors for the performance of oil-injected RPDC by means of combined qualitative visualizations and integral torque measurements. Patel *et al.* [4] measured the temperature field inside an oil-free RPDC by means of laser-induced fluorescence (LIF), which was later complemented with planar – i.e. two dimensional & two component (2D2C) – particle image velocitmetry (PIV) in the annular housing-gap plane of the RPDC by the same group [5]. Since additional knowledge of the lateral distribution of flow field across the annular housing gap is

Content from this work may be used under the terms of the Creative Commons Attribution 4.0 licence. Any further distribution of this work must maintain attribution to the author(s) and the title of the work, journal citation and DOI.
Published under licence by IOP Publishing Ltd

of utmost importance to improve both prediction and optimization strategies towards advanced RPDC efficiency, volumetric (3D3C) flow-diagnostics approaches seem mandatory for the given two-phase flow scenario.

Tomographic PIV [6] and more recently also Lagrangian particle tracking (LPT) methods [7] enjoy increasing attention for quantitative 3D3C flow diagnostics. However, these volumetric standard approaches might have limited applicability in cases, where microscopic characteristic length scales such as e.g. the cross-section of micro channels or - in the present context - a thin housing gap are accompanied by macroscopic characteristic lengths scales along the channel-flow direction or the lateral surface, respectively. For such wide aspect-ratio flow scenarios defocused imaging approaches [8] provide a promising alternative, where size and/or shape of the defocused particle image (PI) rather than the multi-camera tomographic reconstruction provides information on the depth location of the PI along the optical axis imaging setup inside the measurement volume. In context of planar thin gap flows, Leister *et al.* [9, 10] recently analyzed the single-phase flow scenario inside 400-540 µm wide rotor-stator gaps of an open wet clutch experimentally by means of phase-resolved defocusing particle tracking velocimetry (DPTV). This study furthermore took advantage of the known no-slip boundary conditions at rotor and stator to apply an in-situ calibration approach [11, 12].

In addition to a DPTV-based evaluation of the liquid phase, in case of RPDCs, additional complementary diagnostics of the two-phase character of investigated flow is mandatory. Standard (high-speed) imaging approaches by means of reflected light processes are suitable for macroscopic sizing and tracking efforts of liquid-gas interfaces, where small-scale processes such as bubble onset and initial growth require additional diagnostics approaches. For such disperse cases e.g. the interferometric particle imaging (IPI) is a promising approach for image-based particle-size analysis [13], which has been repeatedly applied for both spray-characterization [14] and bubble-sizing studies [15, 16].

The general applicability of both DPTV and IPI for two-phase flow diagnostics in thin annular gaps has recently been successfully outlined by Leister *et al.* [17], where the measurement system was operated in side-scatter configuration - i.e. optical axes of laser and camera were oriented approximately perpendicular. To prepare for the limited optical access of e.g. RPDC-related investigations, Leister *et al.* [10] successfully conducted back-scatter DPTV measurements through a transparent disc. Likewise, Sax *et al.* [18] evaluated and testified the applicability of IPI in back-scatter orientation in a combined theoretical/experimental investigation. Both studies [10, 18] only considered planar surfaces for the optical access, which accordingly resulted in circular particle images (PI).

The curved boundaries of the annular housing gap of RPDCs introduce additional astigmatism to the optical transfer function (OTF) of the experimental approach. As concluded by Leister *et al.* [17], the corresponding shape deformation of the recorded defocused PIs is hypothesized to provide additional information for the depth localization, which might take additional advantage of established astigmatism particle image velocimetry (APTV) approaches [19, 20].

In continuation of earlier studies by Leister *et al.* [17] the purpose of the present study is the adaption of the OTF towards a combined APTV/DPTV evaluation of RPDC-related gap-flow diagnostics. Since the measurement volume inside the above-mentioned boundary curvature accordingly acts as a cylinder lens itself, no immediate application of standard APTV approaches [19, 20] is straight-forwardly possible. Consequently, a quantitative characterization of the experimental optical system including the surface curvature will be elaborated for the PI localization in a first step. Subsequently, the developed OTF is testified with a first set of manually labeled raw data originating from both DTPV and IPI PIs, where the vertical and horizontal axes of the PIs (respectively corresponding to the vertical and azimuthal cylinder axes) are compared. Also the resulting particle displacements are determined to comparatively

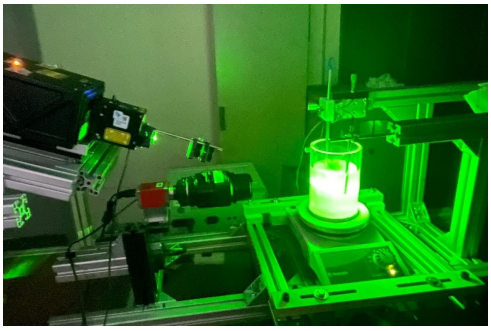

(a) experimental setup, photography

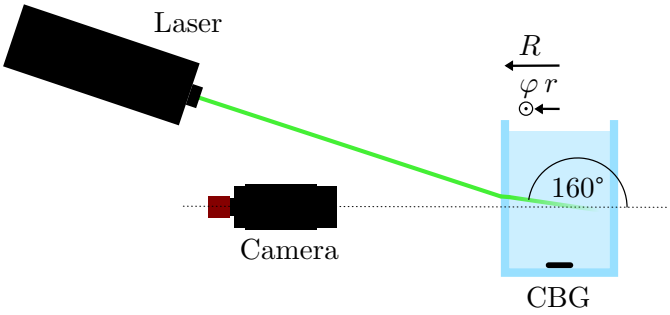

(b) experimental setup, sketch

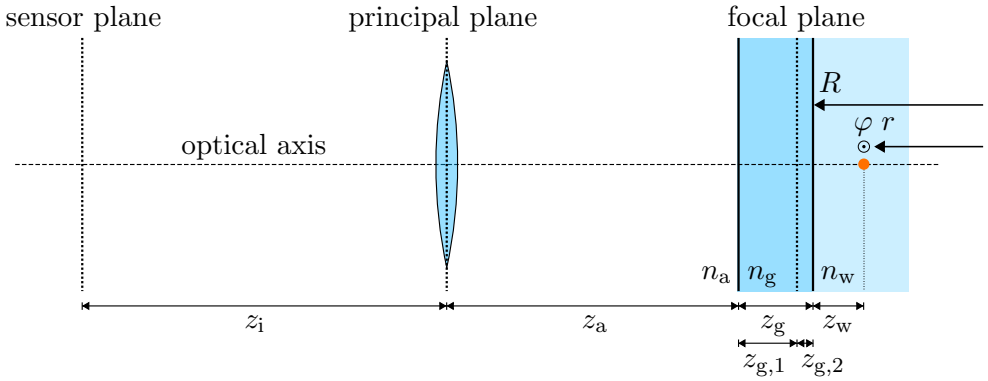

(c) optical configuration and geometric distances; focal plane within glass for sufficiently defocused particle images

Figure 1. Experimental setup, photography (a) and sketch (b), optical configuration (c) of the experimental and processing procedure for the IPI and DPTV evaluations.

evaluate the theoretical (present OTF) and the retroactively determined [11, 12] no-slip PI diameter at the wall of the utilized circular beaker glass (CBG).

2. Experimental and Processing Procedure

2.1. Experimental setup

The experimental setup is comprised of a CBG (inner diameter $2R = 88.9\,\text{mm}$, wall thickness $z_g = 5.8\,\text{mm}$, acrylic glass refractive index $n_g = 1.492$), which sits on a magnetic stirrer to maintain a circumferential velocity of the water (density $\varrho_w = 993\,\text{kg/m}^3$, dyn. viscosity $\mu_w = 6.5 \times 10^{-4}\,\text{kg/ms}$ at $40°C$, refractive index $n_w = 1.333$); see Figure 1(a). The water is seeded with 20 µm diameter Polyamid particles (density 1150 kg/m^3) for the DPTV evaluation, which results in a particle response time of $\tau_p \approx 34\,\mu\text{s}$ and a correspondingly small Stokes number $St < 10^{-2}$ for the tracer-based velocimetry [21]. Note, however, that upon sufficient displacement from the focal plane the particle diameter itself no longer contributes to the diameter of the PI; see e.g. the treatise of Olsen & Adrien [22]. Furthermore, the electrolysis apparatus as already used by Sax *et al.* [18] is applied to produce a constant rate of bubbles for the IPI approach. A *PCO Pixelfly* camera (14 bit, maximum resolution 1392 × 1040 pixels) is equipped with an $f = 105\,\text{mm}$ *Nikon Nikkor* lens to capture both classes of PIs. The CBG is illuminated with the raw beam of a *Quantel EverGreen* Nd:YAG ($\lambda = 532\,\text{nm}$, 200 mJ) dual-cavity laser, which is oriented vertically in 160° back-scatter orientation to ensure reasonable IPI fringe-pattern visibility in back-scatter mode [18]. Double frame images are recorded at 15 Hz repetition rate with a pulse distance between the laser cavities of $\Delta t = 300\,\mu\text{s}$.

Table 1. Experimental and optical parameters

Quantity	**Value**
focal length f	105 mm
f-number $f_\#$	2.8
aperture diameter $D_\mathrm{a} = f/f_\#$	37.5 mm
magnification M	1.06
reproduction scale	6.1 µm/px
camera sensor pixel size	6.45 µm
refractive index air n_a	1
refractive index acrylic glass n_g	1.492
refractive index water n_w	1.333
thickness beaker glass wall z_g	5.8 mm
time interval Δt between frame A and B	300 µs

2.2. Optical considerations

Sufficiently displaced from the focal plane, the defocused particle image diameter a can be approximated as proportional to the optical distance z^* to the focal plane as e.g. elaborated in the treatise of Olsen & Adrian [22]. This assumption has been shown to hold true for the present class of defocus applications [9–12]. Accordingly, the combination of defocus sensitivity $\partial z/\partial a$ (change of particle depth position with particle image size, see also Equation 11) and the PI diameter at the glass-water interface $a(R)$ are the desired quantities for the OTF of the setup. The optical configuration of the imaging system is sketched in the vertical plane in Figure 1(c). Note that this plane serves as basis for the OTF, since no additional astigmatism is introduced in this plane, which in turn lead to robust estimates of the expected vertical PI axis a_v (minor axis of the elliptical PI). The horizontal axis a_h of the defocused PI (major axis of the elliptical PI), in contrast, will be influenced by the astigmatism caused by the curved beaker glass surface.

Focal length ($f = 105\,\mathrm{mm}$), f-number ($f_\# = 2.8$), camera sensor pixel size (6.45 µm), thickness of the beaker glass wall ($z_\mathrm{g} = 5.8\,\mathrm{mm}$) and the refractive indices of air, acrylic glass and water are known optical parameters. A summary of these and further parameters can be found in Table 1.

As a first step a calibration target is recorded at the glass-water interface to determine the magnification $M = 1.06$ of the optical setup and the reproduction scale of 6.1 µm/px. Considering the definition of magnification [21]

$$M = \frac{z_\mathrm{i}}{z_\mathrm{o}} \tag{1}$$

and focus criterion [21]

$$\frac{1}{f} = \frac{1}{z_\mathrm{i}} + \frac{1}{z_\mathrm{o}}, \tag{2}$$

the image distance $z_\mathrm{i} = 216.3\,\mathrm{mm}$ and the optical object distance $z_\mathrm{o} = 204.1\,\mathrm{mm}$ can be calculated straight forwardly from the determined and subsequently known values for M and f [21] . Since the object distance z_o is comprised of both traveled distance in air and the known contribution inside the glass, i.e.

$$z_\mathrm{o} = \frac{z_\mathrm{a}}{n_\mathrm{a}} + \frac{z_\mathrm{g}}{n_\mathrm{g}}, \tag{3}$$

the distance between principal plane and air-glass interface can be determined as $z_\mathrm{a} = 200.2\,\mathrm{mm}$, cp. also Figure 1(c).

In order to obtain sufficiently defocused particle images at the glass-water interface and beyond, the camera is moved backwards by 600 µm after imaging the calibration target. This

results in a modified value for $z_a = 200.8\,\text{mm}$, with the focal plane now situated within the glass; see Figure 1(c). The geometric location of the focal plane inside the glass is

$$z_{g,1} = \left(z_o - \frac{z_a}{n_a} \right) \cdot n_g = 4.9\,\text{mm} \tag{4}$$

for the distance between the air-glass interface to the focal plane and likewise the distance to the glass-water interface $z_{g,2} = z_g - z_{g,1} = 0.9\,\text{mm}$. The optical distance for a particle at the glass-water interface can then be determined as

$$\frac{z_a}{n_a} + \frac{z_g}{n_g} = 204.7\,\text{mm}. \tag{5}$$

According to Olsen & Adrian [22] the vertical axis a_v of a PI can be calculated by

$$a_v = \sqrt{\underbrace{M^2 d_p^2}_{\text{geometric image}} + \underbrace{5,95(M+1)^2 \lambda^2 f_\#^2}_{\text{diffraction}} + \underbrace{\frac{M^2 z^{*2} D_a^2}{(z_o + z^*)^2}}_{\text{defocusing}}}, \tag{6}$$

with the particle size d_p, the laser wavelength λ and the aperture diameter $D_a = f/f_\# = 37.5\,\text{mm}$. For sufficient defocusing (sufficiently large z^*) and a large optical distance between focal plane and principal plane z_o in comparison to the particle's optical distance to the focal plane z^* the equation simplifies to

$$a_v = \frac{M D_a}{z_o} z^*, \tag{7}$$

because the geometric image term and the diffraction term become negligible compared to the defocusing term [10]. Note that for sufficiently defocused particle images as generally applies for DPTV, particle size accordingly has negligible influence on the resulting PI size.

For the optical distance

$$z^* = \frac{z_{g,2}}{n_g} = 0.6\,\text{mm}, \tag{8}$$

the vertical axis of PIs at the glass-water interface can now be determined via Equation 7, which results in $a_v = 116.85\,\mu\text{m}$. For any particle beyond the glass-water interface, z^* expands to

$$z^* = \frac{z_{g,2}}{n_g} + \frac{z_w}{n_w}, \tag{9}$$

which likewise also modifies the vertical PI diameter inside the CBG to

$$a_v(z_w) = \frac{M D_a}{z_o} \left(\frac{z_{g,2}}{n_g} + \frac{z_w}{n_w} \right). \tag{10}$$

Note that the optical distance z_w in the water can be also translated into a CBG-fixed frame of reference, where the radial particle location r and its distance to the outer wall z_w can be converted via $z_w = R - r$; see Figure 1(c).

The determination of the defocus sensitivity can be approximated via the slope of Equation 10, i.e.

$$\frac{\partial z}{\partial a} = \frac{\Delta z_w}{\Delta a_v} = \frac{z_o n_w}{M D_a}, \tag{11}$$

where Δz_w is the displacement of a particle along the optical axis and Δa_v the corresponding change in the PI's vertical axis. For the given experimental configuration the defocusing sensitivity and vertical axis for particles at the glass-water interface are finally determined to $44\,\mu\text{m/px}$ and $a_v(z_w = 0) = 18.12\,\text{px}$.

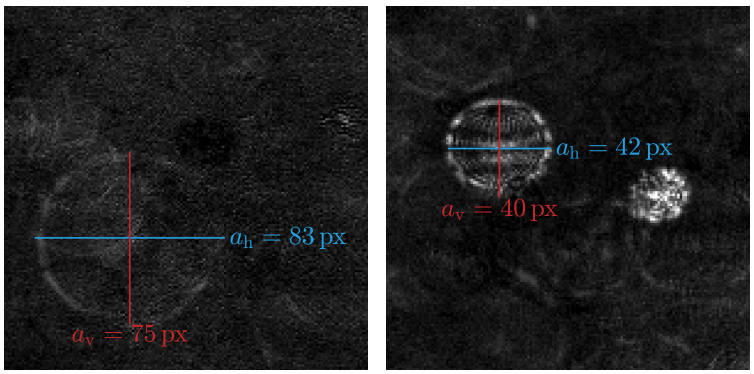

(a) preprocessed DPTV result (b) preprocessed IPI result

Figure 2. Random PIs of the recorded tracer particles (a) and bubbles (b); manually labeled vertical and horizontal axes a_v and a_h are added to either PI in red and blue to the pre-processed images, respectively.

3. Results

Random results of both classes of recorded PIs are shown in Figure 2, which already comprise the manually-labeled vertical (red) and horizontal (blue) axes, a_v and a_h, of the ellipsoidal PIs. Note that the different PI light intensities between Figure 2(a) and 2(b) indicate the general competing effect of PI diameter and resulting signal-to-noise (SNR) ratio for a given scatter-light intensity (cp. also Leister *et al.* [10] in context of circular PIs).

To evaluate the impact of astigmatism originating from the CBG curvature on the resulting PI shape, both axes of the 342 manually labeled PIs of tracer particles (DPTV, green) and bubbles (IPI, red) are plotted against one another in Figure 3. Furthermore, a bisecting dashed line is added to the diagram to indicate the case of circular PIs as reference slope for the evaluation of the additional effect of astigmatism. As expected from the theoretical considerations in Section 2.2 no PI diameters below $a_v = 18.12\,\text{px}$ are registered, which retroactively confirms the applicability of the above approach. Moreover, the slope of the distribution of registered PI diameters falls considerably below the dashed reference. The resulting slope for the PIs is determined from a linear regression and also added to the diagram to have immediate comparability to the circular reference. This diminished slope is observed to likewise hold true for both classes of PIs, i.e. tracer particles (DPTV) and bubbles (IPI), which further confirms the independence of the combined defocus/astigmatism effect on the particle class.

A combined depth-codification and velocity estimation is displayed in Figure 4, where the horizontal PI displacement between two consecutive frames A and B of a double-frame image is shown against the vertical PI diameter a_v (both in pixels). A linear regression of the scattered data is added to the diagram with fixed no-slip boundary condition at the wall, i.e. zero displacement for $a_v = 18.12\,\text{px}$ as indicator for the expected quasi-linear near-wall velocity profile (cp. Leister *et al.* [17]). The scatter margin ($\approx 3\,\text{px}$) of the data points indicates the limited accuracy of the manually conduced labeling approach of the registered PIs. Nonetheless, the scattered results clearly reveal the expected slope of particle displacements. In order to convert the diagram also into physical coordinates, a second abscissa is added at the top of the diagram, which shows the wall distance $z_w = R - r = \frac{\Delta z_w}{\Delta a_v} a_v$. Similarly, the determined PI displacements are converted to circumferential velocities $u_\varphi(z_w)$ via reproduction scale and laser pulse distance, which reasonably resemble the expected velocity range for the stirred water in the CBG.

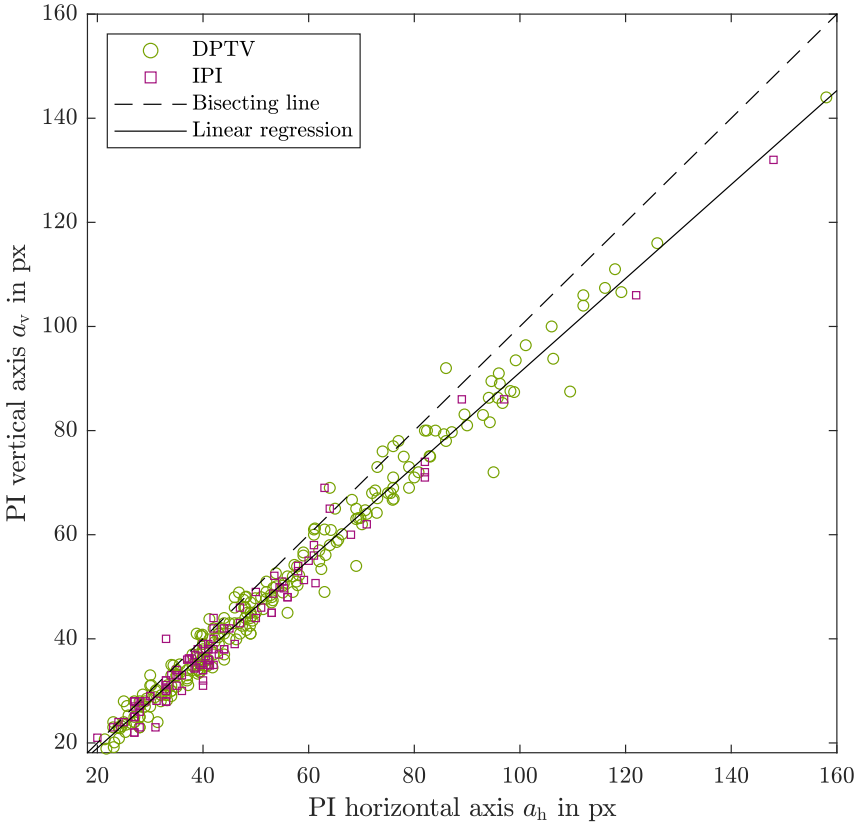

Figure 3. Evaluation of PI size and shape upon the combined influence of defocussing and astigmatism effects for 342 manually labeled particle images: The ordinate shows the vertical axis a_v, which only contains the imprint of defocussing, the abscissa shows the horizontal axis a_h, which furthermore comprises the stretching effect of astigmatism. A bisecting dashed line indicates the slope of circular PIs as reference for the linear regression of the registered PIs (solid line) the latter revealing a diminished slope.

4. Concluding Remarks

In continuation of earlier efforts towards quantitative laser-optical back-scatter diagnostics of the annular two-phase flow in RPDCs [10, 17, 18] the presented combined theoretical and experimental study addresses additional optical considerations as inevitably occurs for imaging measurements across curved surfaces. To mimic the impact of astigmatism on the OTF of the experimental approach, a CBG of comparable diameter as apply for typical RPDCs is chosen for the measurements, which reveals a mild yet significant impact of the curved surface on the resulting shape deformation of the recorded PIs. The correspondingly distinctively different defocus-sensitivity slopes for horizontal and vertical axes are, therefore, hypothesized to provide additional quantitative depth localization measures.

The derivation of the underlying OTF for the given problem comprises the three separate contributions of the air between the imaging equipment and the glass wall, the thickness of the wall, and the depth location inside the flow domain. Consequently, this OTF is straightforwardly applicable for future experimental efforts of similar geometrical/optical configurations. Moreover, the defocus PI-diameter determination for the no-slip condition at

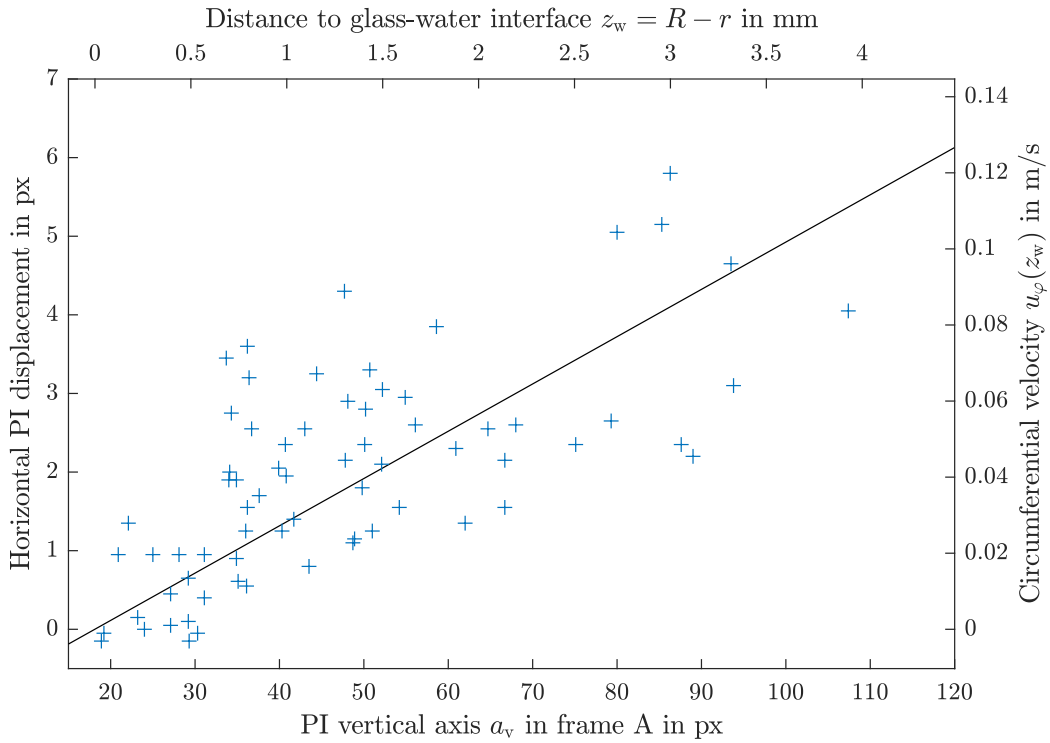

Figure 4. Particle-displacement evaluation for PI pairs. The lower and upper abscissae respectively show the vertical PI diameter a_v and correspondingly determined physical depth localization $z_w = R - r$. The latter can be calculated from Equation 10 as explained in Section 2.2; the left ordinate reveal the horizontal PI displacement in pixels between two consecutive frames A and B of a double-frame image; the right ordinate reveals the circumferential velocity $u_\varphi(z_w)$ of the respective particles as function of wall distance $z_w = R - r$. The two ordinates are equivalent and can be transformed into one another through the application of reproduction scale and time interval Δt. A linear regression of measured data is added to the diagram with fixed no-slip boundary condition at the wall.

the wall-liquid interfaces is shown to provide valuable a-priori information for the calibration of particle displacement curves. To improve the calibration procedure further, it seems promising to further merge the present OTF-based a-priori approach with both in-situ calibration [11,12] but also a purpose-developed calibration image stack for the so-called general defocusing particle tracking (GDPT) [23, 24]. The latter is foreseen to also take immediate advantage of the development of the above-mentioned different defocus sensitivity slopes for horizontal and vertical axes.

As a final remark, the present study demonstrates the combined and simultaneous applicability of DPTV and IPI in backscatter configuration for the investigation of RPDC-related two-phase gap flows. However, to advance beyond the present proof-of-concept level, more sophisticated conventional and also machine-learning (ML) assisted pattern-identification approaches seem mandatory, which is indicated through the considerably scattered data margin of the presented results. Similar to ring detection in DPTV [25, 26], in this context current efforts at ISTM also center around an ML-based detection and classification of DPTV and IPI result, where the experimental results of the present study represent a preliminary subset of labeled ground-truth information for the supervised learning process.

Acknowledgments
This work was funded by the Deutsche Forschungsgemeinschaft (DFG, German Research Foundation) via Project Grant KR4775/4-1 within the Research Unit FOR 5595 Archimedes (Oil-refrigerant multiphase flows in gaps with moving boundaries — Novel microscopic and macroscopic approaches for experiment, modeling, and simulation) — Project Number 510921053.

References
[1] Nikolov A and Brümmer A 2023 Two-phase mass flow rate through restrictions in liquid-flooded twin-screw compressors or expanders *International Journal of Refrigeration* **148** 152–167 URL https://doi.org/10.1016/j.ijrefrig.2023.01.017
[2] Xin D, Feng J, Jia X and Peng X 2010 An investigation into oil—gas two-phase leakage flow through micro gaps in oil-injected compressors *Proceedings of the Institution of Mechanical Engineers, Part C: Journal of Mechanical Engineering Science* **224** 925–933 URL https://doi.org/10.1243/09544062JMES1704
[3] Vasuthevan H and Brümmer A 2019 Generic experimental investigation of hydraulic losses within twin-screw machines *The 9th International Conference on Compressor and Refrigeration.* **Xi'an (China)** 10pp
[4] Patel B, Kovacevic A, Charogiannis A, Alam M N and Schütte M 2021 The use of laser-induced fluorescence to measure temperature in the leakage gaps of oil-free positive displacement rotary machines *Measurement* **185** 110057 URL https://doi.org/10.1016/j.measurement.2021.110057
[5] Patel B, Kovacevic A, Plantegenet T and Tam T 2023 Study of leakage flow in oil-free positive displacement rotary machines using particle image velocimetry *Experimental Thermal and Fluid Science* **145** 110886 URL https://doi.org/10.1016/j.expthermflusci.2023.110886
[6] Scarano F 2013 Tomographic piv: principles and practice *Measurement Science and Technology* **24** 012001 URL https://dx.doi.org/10.1088/0957-0233/24/1/012001
[7] Schröder A and Schanz D 2023 3D lagrangian particle tracking in fluid mechanics *Annual Review of Fluid Mechanics* **55** 511–540 URL https://dx.doi.org/10.1146/annurev-fluid-031822-041721
[8] Barnkob R, Kähler C J and Rossi M 2015 General defocusing particle tracking *Lab on a Chip* **15** 3556–3560 URL https://doi.org/10.1039/C5LC00562K
[9] Leister R, Fuchs T, Mattern P and Kriegseis J 2021 Flow-structure identification in a radially grooved open wet clutch by means of defocusing particle tracking velocimetry *Experiments in Fluids* **62** 29 URL https://doi.org/10.1007/s00348-020-03116-0
[10] Leister R, Fuchs T and Kriegseis J 2023 Defocusing ptv applied to an open wet clutch: From macro to micro *Experiments in Fluids* **64** 94 URL https://doi.org/10.1007/s00348-023-03623-w
[11] Fuchs T, Hain R and Kähler C J 2016 In situ calibrated defocusing ptv for wall-bounded measurement volumes *Measurement Science and Technology* **27** 084005 URL https://doi.org/10.1088/0957-0233/27/8/084005
[12] Fuchs T, Hain R and Kähler C J 2016 Uncertainty quantification of three-dimensional velocimetry techniques for small measurement depths *Experiments in Fluids* **57** 73 URL https://doi.org/10.1007/s00348-016-2161-5
[13] Tropea C 2011 Optical particle characterization in flows *Annual Review of Fluid Mechanics* **43** 399–426 URL https://doi.org/10.1146/annurev-fluid-122109-160721
[14] Fansler T D and Parrish S E 2014 Spray measurement technology: a review *Measurement Science and Technology* **26** 012002 URL https://doi.org/10.1088/0957-0233/26/1/012002
[15] Dehaeck S and van Beeck J 2008 Multifrequency interferometric particle imaging for gas bubble sizing *Experiments in Fluids* **45** 1432–1114 URL https://doi.org/10.1007/s00348-008-0502-8
[16] Kawaguchi T, Akasaka Y and Maeda M 2002 Size measurements of droplets and bubbles by advanced interferometric laser imaging technique *Measurement Science and Technology* **13** 308–316 URL https://doi.org/10.1088/0957-0233/13/3/312
[17] Leister R, Brümmer A and Kriegseis J 2022 Laser-optical shear-flow analysis across the annular gap of a simplified displacement compressor model *IOP Conference Series: Materials Science and Engineering* **1267** 012003 URL https://doi.org/10.1088/1757-899X/1267/1/012003
[18] Sax C, Dreisbach M and Kriegseis J 2023 Interferometric particle imaging for particle sizing in the front-, side-, and back-scatter region *arXiv preprint arXiv:2303.16013* URL https://doi.org/10.48550/arXiv.2303.16013
[19] Cierpka C, Rossi M, Segura R and Kähler C J 2011 On the calibration of astigmatism particle tracking velocimetry for microflows *Measurement Science and Technology* **22** 015401 URL https://doi.org/10.1088/0957-0233/22/1/015401

[20] Rossi M and Kähler C J 2014 Optimization of astigmatic particle tracking velocimeters *Experiments in Fluids* **55** URL https://doi.org/10.1007/s00348-014-1809-2
[21] Raffel M, Willert C E, Scarano F, Kähler C J, Wereley S T and Kompenhans J 2018 *Particle Image Velocimetry* (Springer-Verlag GmbH) URL https://doi.org/10.1007/978-3-319-68852-7
[22] Olsen M G and Adrian R J 2000 Out-of-focus effects on particle image visibility and correlation in microscopic particle image velocimetry *Experiments in Fluids* **29** S166–S174 URL https://doi.org/10.1007/s003480070018
[23] Barnkob R and Rossi M 2020 General defocusing particle tracking: fundamentals and uncertainty assessment *Experiments in Fluids* **61** 110 URL http://dx.doi.org/10.1007/s00348-020-2937-5
[24] Barnkob R and Rossi M 2021 Defocustracker: A modular toolbox for defocusing-based, single-camera, 3d particle tracking *Journal of Open Research Software* **9** 22 URL https://doi.org/10.5334/jors.351
[25] Dreisbach M, Leister R, Probst M, Friederich P, Stroh A and Kriegseis J 2022 Particle detection by means of neural networks and synthetic training data refinement in defocusing particle tracking velocimetry *Measurement Science and Technology* **33** 124001 URL http://dx.doi.org/10.1088/1361-6501/ac8a09
[26] Sax C, Dreisbach M, Leister R and Kriegseis J 2023 Deep learning and hybrid approach for particle detection in defocusing particle tracking velocimetry *Measurement Science and Technology* **34** 095909 URL http://dx.doi.org/10.1088/1361-6501/acd4b4